11-1-2006

Storm-time configuration of the inner magnetosphere: Lyon-Fedder-Mobarry MHD code, Tsyganenko model, and GOES observations

Chia-Lin L. Huang
hcl@guero.sr.unh.edu

Harlan E. Spence
Boston University, harlan.spence@unh.edu

J. G. Lyon

F. R. Toffoletto

H. J. Singer

See next page for additional authors

Authors

Chia-Lin L. Huang, Harlan E. Spence, J. G. Lyon, F. R. Toffoletto, H. J. Singer, and S. Sazykin

Storm-time configuration of the inner magnetosphere: Lyon-Fedder-Mobarry MHD code, Tsyganenko model, and GOES observations

Chia-Lin Huang,[1] Harlan E. Spence,[1] John G. Lyon,[2] Frank R. Toffoletto,[3] Howard J. Singer,[4] and Stanislav Sazykin[3]

[1]   We compare global magnetohydrodynamic (MHD) simulation results with an empirical model and observations to understand the magnetic field configuration and plasma distribution in the inner magnetosphere, especially during geomagnetic storms. The physics-based Lyon-Fedder-Mobarry (LFM) code simulates Earth's magnetospheric topology and dynamics by solving the equations of ideal MHD. Quantitative comparisons of simulated events with observations reveal strengths and possible limitations and suggest ways to improve the LFM code. Here we present a case study that compares the LFM code to both a semiempirical magnetic field model and to geosynchronous measurements from GOES satellites. During a magnetic cloud event, the simulation and model predictions compare well qualitatively with observations, except during storm main phase. Quantitative statistical studies of the MHD simulation shows that MHD field lines are consistently under-stretched, especially during storm time ($Dst < -20$ nT) on the nightside, a likely consequence of an insufficient representation of the inner magnetosphere current systems in ideal MHD. We discuss two approaches for improving the LFM result: increasing the simulation spatial resolution and coupling LFM with a ring current model based on drift physics (i.e., the Rice Convection Model (RCM)). We show that a higher spatial resolution LFM code better predicts geosynchronous magnetic fields (not only the average B_z component but also higher-frequency fluctuations driven by the solar wind). An early version of the LFM/RCM coupled code, which runs so far only for idealized events, yields a much-improved ring current, quantifiable by decreased field strengths at all local times compared to the LFM-only code.

Citation: Huang, C.-L., H. E. Spence, J. G. Lyon, F. R. Toffoletto, H. J. Singer, and S. Sazykin (2006), Storm-time configuration of the inner magnetosphere: Lyon-Fedder-Mobarry MHD code, Tsyganenko model, and GOES observations, *J. Geophys. Res.*, *111*, A11S16, doi:10.1029/2006JA011626.

1.   Introduction

[2]   The inner magnetosphere is most dynamic during magnetic storm intervals. This dynamism is characterized by various phenomena, including disturbances in the auroral zone, radiation belt activity, ring current formation, and worldwide ground magnetic field fluctuations. Understanding storm time features and their time evolution will be beneficial for describing the disturbed space environment and for assessing space weather effects. From another perspective, describing the innermost magnetosphere is important to provide inner boundary constraints to global magnetospheric models.

[3]   Theories and observations have revealed many of the interesting physical interactions that couple the solar wind, magnetosphere, and ionosphere system. However, modeling this time-varying, coupled system and predicting Earth's space weather are still under development. The plasma sources, particle energization, and transport mechanisms in the inner magnetosphere remain unclear, thus limiting our ability to simulate the evolution of magnetic field topology and plasma distribution during magnetic storms. In addition, limited computational resources constrain numerical modelers to simulate these regions using simplifying assumptions.

[4]   Comprehensive, global magnetospheric models simulate Earth's magnetosphere. There are two major categories of these global models: data-based empirical models and MHD physics-based numerical simulations. The series of

---

[1]Center for Space Physics, Boston University, Boston, Massachusetts, USA.
[2]Department of Physics and Astronomy, Dartmouth College, Hanover, New Hampshire, USA.
[3]Physics and Astronomy Department, Rice University, Houston, Texas, USA.
[4]Space Environment Center, NOAA, Boulder, Colorado, USA.

Tsyganenko models [*Tsyganenko*, 1987, 1989, 1995, 2002a, 2002b; *Tsyganenko et al.*, 2003; *Tsyganenko and Sitnov*, 2005], developed over the past two decades, are semi-empirical magnetospheric field models. The community uses them broadly for various applications, largely because they are easy to use and more readily available to users. These models rely on sometimes sparsely sampled data, so testing the models under different conditions and then quantifying their strengths and limitations is beneficial for model users. With increasing computational capabilities available recently, global MHD simulations are now a practical higher-level tool to explore the global, dynamic space environment [*Janhunen and Huuskonen*, 1993; *Ogino et al.*, 1994; *Winglee*, 1998; *Raeder*, 1999; *Powell et al.*, 1999; *White et al.*, 2001; *Tanaka*, 2003; *Lyon et al.*, 2004; *Toth et al.*, 2005]. Despite the limitations inherent to ideal MHD, the global MHD codes describe the magnetosphere reasonably well, but not always perfectly. In this paper, we explore the ability of the Lyon-Fedder-Mobbary (LFM) MHD code [*Lyon et al.*, 2004] to predict the inner magnetosphere environment during geomagnetic storm events.

[5] Accurately modeling the time-dependent global magnetic field is important for understanding the microscopic and macroscopic behavior of charged particles in the inner magnetosphere. During magnetic storm intervals, the dramatic change of magnetic fields in the inner magnetosphere is presently very difficult to predict, both in empirical models and in MHD simulations. Models that simulate time-dependent variations of the plasmasphere, ring current, and radiation belt all use time-dependent global magnetic fields as inputs, and these fields can significantly alter model results [*Moldwin et al.*, 2002; *Toffoletto et al.*, 2004; *Elkington et al.*, 2004]. As the inner magnetosphere magnetic field configuration changes during active periods, charged particles redistribute quickly and broadly [*Reeves et al.*, 2005]. Consequently, verifying the accuracy of these global field models under different conditions is essential to many related modeling efforts in the inner magnetosphere. In addition, quantifying model performance provides crucial information for future model improvement.

[6] Several studies [*Thomsen et al.*, 1996; *Pulkkinen*, 2001] tested early versions of the Tsyganenko models (*Tsyganenko* [1989, 1995], respectively), by comparing the model outputs with magnetic field measurements from GOES satellites. These studies showed that the Tsyganenko models predict the field strength at geosynchronous orbit reasonably well for long-term variations. However, the earlier models over-stretch magnetic field lines on the nightside during both quiet and disturbed periods. Recently, Tsyganenko developed new model versions that use larger data sets and better algorithms. Full evaluation in the published literature of these recent models [*Tsyganenko*, 2002a, 2002b; *Tsyganenko et al.*, 2003] has not yet occurred.

[7] The Geospace Environment Modeling (GEM) grand challenges successfully coordinated a broad range of computational models to assess the models' capabilities to reproduce and explain aspects of substorm event and magnetic reconnection [*Birn et al.*, 2001; *Raeder et al.*, 2001; *Ridley et al.*, 2002]. For the LFM code, validation efforts have taken two forms: case studies and statistical. For example, simulation outputs have been compared with

magnetic field observations for single event studies [*Fedder et al.*, 1997; *Goodrich et al.*, 1998; *Pulkkinen and Wiltberger*, 2000] and also with long-term plasmasheet flow patterns derived from years of Geotail measurements [*Guild et al.*, 2004]. While common features exist between the simulated results and observations in the latter study, there are also some differences. *Guild et al.* [2004] proposed that the lack of gradient and curvature drift physics in the LFM code explains the discrepancy between simulation results and satellite observations.

[8] In this paper we present a comprehensive study of the LFM code, the Tsyganenko storm model [*Tsyganenko et al.*, 2003], and GOES observations during magnetic storm intervals. We compare the simulation- and model-predicted fields with geosynchronous measurements for a major storm event. We explore global features of these models by comparing the magnetic field configurations, current systems, and pressure gradients at storm main phase. In the discussion session, we quantify the MHD code degree of accuracy over a long-term simulation interval. Finally, we suggest several possible methods to improve model performance and explore them qualitatively and quantitatively. In sum, the goals of this study are, first, to understand the global structure and dynamical evolution of the inner magnetosphere field and plasma during magnetic storms, and second, to quantify and compare the ability of the LFM code and Tsyganenko storm model to reproduce the storm time magnetosphere.

2. LFM MHD Code

[9] Global MHD modeling is a valuable and powerful tool for exploring the vast and complex geospace environment. The Lyon-Fedder-Mobbary (LFM) code used in our study is one of the major three-dimensional MHD codes used to simulate Earth's magnetosphere [*Lyon et al.*, 2004; *Wiltberger et al.*, 2004]. The simulation domain spans 30 R_E upstream to 300 R_E downstream in the X direction, and +100 to −100 R_E in the Y and Z directions. The simulations use solar wind data from satellites (e.g., Wind or ACE) as the upstream boundary condition. They solve the MHD equations using a total variation diminishing scheme [*Lyon et al.*, 2004]. A special computational grid based on distorted spherical coordinates is used in the simulations, with polar axis aligned with X direction in solar magnetic (SM) coordinates. The grid is distorted in the radial and polar directions to allow finer resolution in regions of interest such as the magnetopause, bow shock, inner magnetosphere, and magnetotail. This grid structure provides finer-scale computation in those regions where gradient-scale lengths are shorter, yet still keeps the simulation time tractable. For a standard resolution run, the number of cells on the radial, azimuthal, and polar axes are 53, 24, and 32, respectively. For detailed definition and information of the LFM grid, please see *Lyon et al.* [2004, Figure 4 and section 3.2]. The radial grid size at geosynchronous orbit is 0.4 R_E on the dayside and 0.5 R_E on the nightside. The azimuthal and polar grid sizes are closer to 1 R_E. The inner boundary of the simulation domain is a 2 R_E radius sphere centered on Earth, where the cell sizes are less than 0.3 R_E. Field-aligned currents (FAC) that flow across the inner boundary map along dipole field lines to a two-dimensional electro-

static ionosphere model. The reduced speed of light used in the Boris correction [*Boris*, 1970] is between 1500 and 3000 km/s for the MHD runs.

[10] Current major global MHD codes are generally similar in many regards. They attempt to reproduce Earth's magnetosphere by solving similar versions of the MHD equations, but typically using different grid structures and numerical methods. Single-fluid MHD cannot fully describe the physics of certain regions in the magnetosphere. Consequently, we need to understand the general limitations of the MHD simulations and use them with caution in such regions.

[11] In the inner magnetosphere there are overlapping particle distributions with a wide range of energies, such as the cold plasmasphere, hot ring current, and energetic radiation belt particles. The MHD simulations solve for a single number density and temperature to represent the magnetospheric plasma. However, a single-fluid characterization is not always sufficient to describe this complicated region. For example, the MHD simulations do not explicitly include gradient and curvature B drifts known to be important for describing the ring current and radiation belt populations. Lack of drift physics in combination with the perfect conductivity assumption may affect the simulation results during storm times, when the ring current builds up rapidly, thus reducing the field strength in the inner magnetosphere. Coupling the LFM MHD code with a ring current model would likely improve the simulation results and early attempts of one such coupling, that is underway, are reported here.

[12] To understand how well the LFM code predicts the storm time inner magnetosphere with these known existing limitations, we validate the simulation results with in situ observations. However, during a single storm event we can only compare the MHD results to satellite data at sparsely sampled points as a function of time. We cannot generally show the global predictive ability of the simulations, except in some limited sense. Therefore we appeal to empirical models in order to supplement our study and compare simulation output throughout a larger volume. A summary of these global empirical models follows below.

3. Tsyganenko Model

[13] The series of Tsyganenko models are empirical magnetic field models. They reproduce the global average of dynamic states of Earth's magnetosphere, based on large quantities of spatially distributed satellite measurements and flexible parameters. The Tsyganenko models have evolved along with the progressive knowledge of space physics. The earliest Tsyganenko models [*Tsyganenko and Usmanov*, 1982; *Tsyganenko*, 1987, 1989] represented the global distribution of the average magnetic field as a function of the Kp index. Over time, the models have improved to include explicit representations of the region 1 and 2 Birkeland current systems, symmetric and partial ring currents, and a warped tail current sheet. Physically relevant quantities, including the upstream solar wind and IMF, and the Dst index, parameterize the current models. The model data-fitting method has also advanced with time, from the amplitude of the external field sources being dependent linearly on solar wind inputs, to nonlinear saturation of

these sources during extreme conditions. Tsyganenko models provide global static views of Earth's magnetosphere which mimic the time-evolving magnetosphere with minimal computer time. However, because these models are data based and because extreme conditions are rare, model users should be especially cautious when using these earlier model versions for large storm events.

[14] The Tsyganenko 2003 model (noted as T03 or T01_S [*Tsyganenko et al.*, 2003]) aptly reproduces the stormy magnetosphere. The magnetic field data set of this recent model includes 37 storm events that occurred between 1996 and 2000, using most of the available satellite data in the inner magnetosphere. In addition to solar wind data and the Dst index, this new model also uses time-integration indices (G2 and G3) as inputs to capture the geomagnetic coupling effects between the solar wind and the magnetosphere. The magnetosphere responds nonlinearly during strongly disturbed intervals, so nonlinear fitting methods treat the saturation characteristics during extreme conditions. Both of the time-integration effects and the nonlinear interpolation of the current calculation limit the growth of the field sources for active conditions. Since the storm event in our study is included in the 2003 model data set, we should expect the T03 model to reproduce this storm very well. Therefore, we chose T03 as our standard baseline empirical model for our MHD comparison on a more global scale.

4. Case Study: Event Description

[15] The storm event we selected for thorough examination is a magnetic-cloud-associated storm during 24–26 September 1998 (denoted as Sep98). It is a storm selected for study by the GEM community and has features of typical major storms. Figure 1 shows the solar wind conditions and the Dst index for this event. The top and middle panels of Figure 1 show solar wind number density, velocity and ram pressure, and IMF components in GSM coordinates, measured by the Wind spacecraft at $\sim$180 R_E upstream (180, 15 and 10 R_E in GSM Cartesian coordinates). Using the Dst index (bottom panel) as an indication of storm event evolution, this event has typical storm features. The solar wind pressure pulse arrived slightly before 25 September and produced a classic storm sudden commencement. A prolonged southward IMF that lasted for approximately 12 hours, which created the large magnetic field disturbance and Dst minimum of -213 nT, followed thereafter. These solar wind data, that span prestorm, storm, storm recovery, and poststorm conditions, serve as inputs for the MHD simulations as well as the Tsyganenko storm model. We compare predictions of these two model magnetospheres with satellite observations.

[16] Magnetic field measurements from geosynchronous satellites provide one test of the predictive skill of both magnetospheric models. NOAA GOES satellites provide continuous magnetic field and energetic particle flux data at geosynchronous orbit. In our case study we use the magnetic field measurements from GOES 8 and 10 to compare with model results. Black curves in Figure 2 and 3 show the GOES data, corrected for the known $\sim$7 and 1 nT offset from the Z component in spacecraft coordinates according to *Tsyganenko et al.* [2003]. We plot the vector components of magnetic field in dipole coordinates. The dipole (or
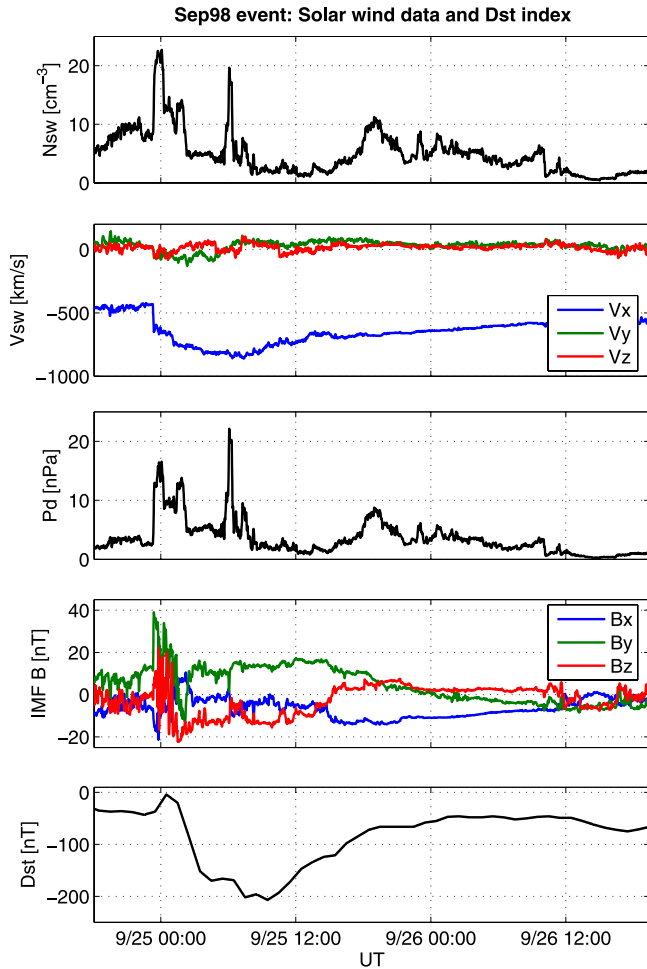
Figure 1. Solar wind conditions for the Sep98 storm event. The top and middle panels show solar wind number density, velocity, and ram pressure, and interplanetary magnetic field (IMF) components in GSM coordinates, measured by the Wind satellite at 180 R_E upstream. The bottom panel shows the *Dst* index.

geomagnetic) coordinate system is defined so that its *Z*-axis is parallel to the magnetic-dipole axis. The *Y*-axis is perpendicular to the geographic poles such that if **D** is the dipole position and **S** is the south pole, $\mathbf{Y} = \mathbf{D} \times \mathbf{S}$. The *X*-axis completes the triad. In this way, changes in each component easily show storm effects in addition to the diurnal variations. The dark circles at the bottom of the panels denote when the GOES 8 and 10 satellites are at local midnight (∼0500 and 0900 UT, respectively). During storm main phase, the B_z component decreased and the B_x component increased in magnitude, indicating that field lines stretch owing to a strong growth of the cross-tail current system.

5.   Quantitative Case Study

[17]   In this section we assess the magnetic field predictions from the LFM code and the Tsyganenko model by comparing with GOES observations during the Sep98 storm event. Because the T03 model included this event in the data set from which it was constructed and because it
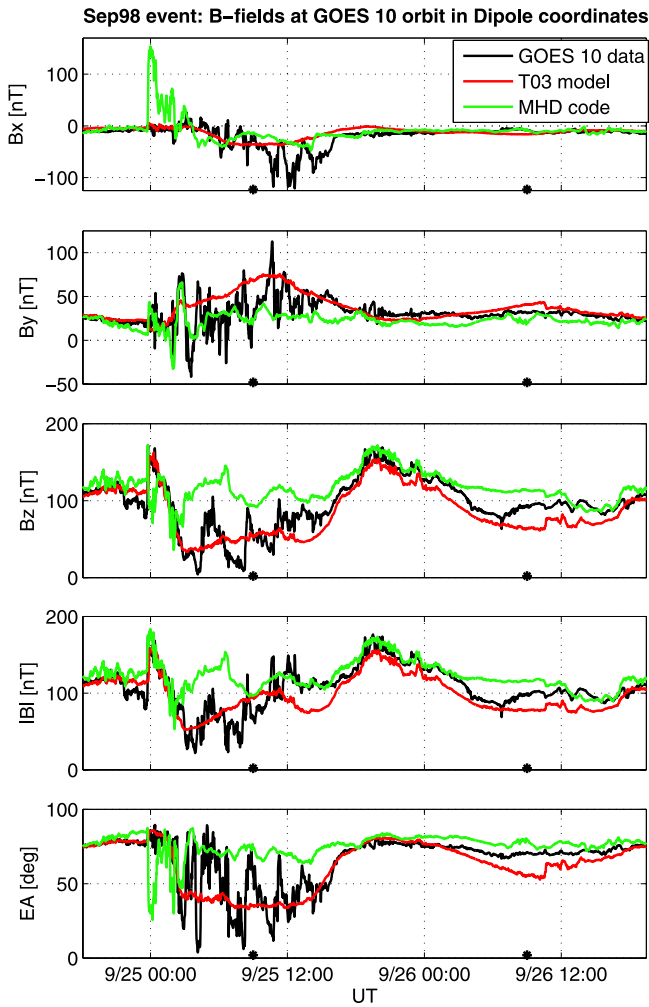
reproduces the magnetic fields at geosynchronous orbit very well, we use it as a proxy to study the global aspects of the LFM code at other locations. We first compare the three-dimensional magnetic field configurations of these two models before the storm and during storm main phase. Then we study the current systems and pressure gradients inferred from both models to understand the differences between the simulated magnetic field structures near the equatorial plane.

5.1.   Comparison With GOES Magnetic Field Measurements

[18]   Figures 2 and 3 show the magnetic field comparisons of GOES 8 and 10 data, the T03 model, and the MHD simulation results during the Sep98 storm event. The top three panels are the vector components of the magnetic field
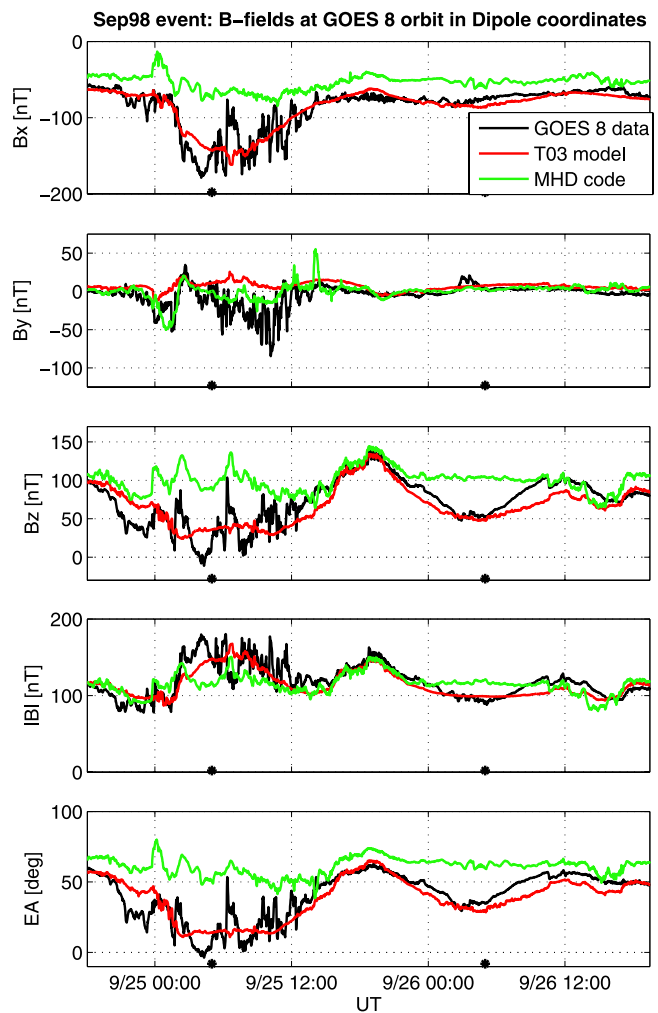
Figure 2. Magnetic field comparisons of data and models during the Sep98 storm event. The black lines are the measurements from GOES 8. The red and green lines are the predicted values of the T03 model and the MHD code at the GOES 8 positions using time-dependent solar wind inputs. The dark circles denote when the GOES 8 satellite is at local midnight. The top three panels are the vector components of the magnetic fields in dipole coordinates. The bottom two panels show the magnetic field magnitude and elevation angle.

Figure 3. The same comparison as Figure 2 using GOES 10 data.

interval, except the *Y* component during storm main phase. The MHD simulations predict lower (higher) magnitude for the *X* (*Z*) component and a good fit for the *Y* component. The MHD simulations are able to reproduce the small time-scale variations driven by the solar wind much better than the T03 model, especially during storm main phase in the *Z* component. In the elevation angle plot, the MHD simulations predict constantly higher angles throughout the event. This indicates the MHD field lines at geosynchronous orbit are not stretched enough compared to observations and the T03 model, especially during storm main phase and on the nightside.

[20] Figure 2 and 3 demonstrate that the LFM code has certain strengths and weaknesses in reproducing magnetic fields of a major magnetic storm at geosynchronous orbit. Comparison with GOES data shows how well the MHD
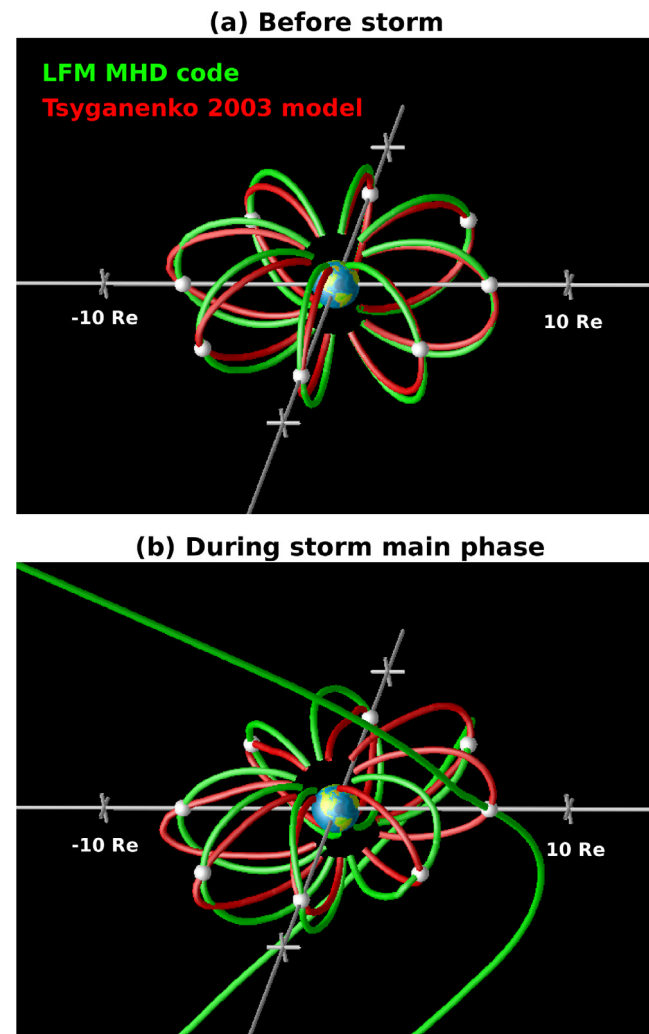
Figure 4. Three-dimensional magnetic field configurations of the T03 model and the MHD simulations, viewed from dawn at an angle above the equator, before storm (top) and during the main phase (bottom). The field lines are traced from points on a 6.6 R_E-radius circle on the GSM equatorial plane, and at eight equispaced local times. The tick marks on the axes are 10 R_E apart and the Sun is toward the right of both panels.

in dipole coordinates and the bottom two panels are the magnetic field magnitude and elevation angle. Elevation angle is defined such that 90 degrees (0 degrees) means the field line is perpendicular (parallel) to the equatorial plane. The black lines are the measurements from GOES satellites after correcting the systematic offset. The red lines are the predicted values of the Tsyganenko storm model at the GOES positions using time-dependent upstream solar wind inputs from the Wind satellite and the *Dst* index. The green lines are the fields predicted by the MHD simulation at the same GOES locations using the same solar wind inputs, except we set IMF B_x to zero for simplicity. The LFM code fields are computed from a standard resolution grid using reduced speed of light of 3000 km/s.

[19] During most of the quiet periods, before the storm and during the recovery phase, the predictions of the MHD simulations and the T03 model agree with the observed fields fairly well. However, the predictions are not as good during the storm main phase (9/25, 0000–1200 UT) and particularly when GOES satellites are on the nightside (9/25 and 9/26 early UT day). In terms of field component magnitudes, the T03 model predicts the storm time magnetic fields better than LFM during most of the storm

simulations predict the field at one point as a function of time, but not its global performance. To investigate the ability of the MHD simulations in reproducing the storm time inner magnetosphere at all local times and throughout the inner magnetosphere, we next study the simulation results globally within the model domain. We know that the T03 model predicts the magnetic field very well at geosynchronous orbit and that it was constructed with and constrained by measurements made throughout the entire inner magnetosphere volume. Therefore we assume that it predicts well everywhere in the inner magnetosphere and use the T03 model as a proxy for global simultaneous observations.

5.2. Comparison of Simulated Field Configurations, Current Systems, and Pressure Gradients

[21] To compare the field topology of both global models, we trace magnetic field lines at all local times. Figures 4a and 4b are three-dimensional magnetic field configurations viewed from dawn at an angle above the equator, before the storm (top panel, 9/24, 1359 UT) and during the main phase (bottom panel, 9/25, 0522 UT). Representative field lines of the MHD simulations (green curves) and the T03 model (red curves) are traced from points on a 6.6 R_E-circle on the GSM equatorial plane, and at eight equispaced local times. The tick marks on the X and Y-axes are 10 R_E apart. The Sun is toward the right in both panels.

[22] Before the storm, the MHD simulations and the T03 model have very similar dipole-like field configurations; the T03 model field lines are only slightly more stretched than the MHD simulation result. During storm main phase, both the MHD and T03 fields stretch more relative to prestorm conditions. However, the MHD magnetic field lines are not as stretched as the T03 model at all local times, especially on the nightside. On the dayside, the MHD open field lines indicate the magnetopause location moves into 6.6 R_E.

[23] We note that we only have confidence in the T03 model predictions where observations (i.e., at geostationary orbit for this event) confirm the model output. Since the occurrence of major storm events (Dst minimum < −200 nT) is low and the data needed to construct empirical models are sparse, it is very difficult to predict empirically the magnetospheric magnetic fields during extreme conditions. Overdriving the parameterized ring current or tail current during large storms can even create artificial sites of reconnected field lines in the inner magnetosphere or unrealistic stretched field lines. To understand more quantitatively field configuration differences between the T03 model and the LFM code, we next explore the near-equatorial current and pressure gradient distributions in these models during storm main phase.

[24] Figures 5a and 5b show the current systems calculated from the T03 model and the MHD simulation at the equatorial plane during the storm main phase (9/25, 0522 UT). Current magnitudes perpendicular to the local magnetic field are shown, calculated from both models by taking the curl of the local magnetic field ($J_\perp = \frac{|(\nabla \times B) \times B|}{\mu_0 |B|}$) according to Ampere's Law (with dE/dt ∼ 0).The color scales of these two current maps are the same and range from 0 to 10 nA/m², with a 1.5 × 1.5 R_E data smoothing. The white dashed lines denote

the location of geosynchronous orbit, centered on Earth. For the MHD simulation, a ring-current-like feature builds up on the nightside during storm main phase, where and when the field lines become more stretched from their original dipole-like shape. Nevertheless, the intensity is too weak to reduce the simulation field strength and yield enough stretching as was observed.

[25] If the models are in magnetohydrostatic equilibrium and the slow flow approximation applies to the inner magnetosphere, then we can assume that the $J \times B$ force balances the plasma pressure gradients. Previous studies showed that Tsyganenko models are approximately consistent with pressure balance [*Spence et al.*, 1987; *Lui et al.*, 1994; *Zaharia and Cheng*, 2003]. Figures 5c and 5d are maps of the plasma pressure gradient ($\nabla P = |J \times B|$) calculated in both models. At geosynchronous orbit, as with the current systems, the MHD simulation has weaker pressure gradients than the T03 model at all local times. Several limitations inherent to the LFM code may contribute to these differences. The MHD simulation does not include ionospheric outflow, which is a major heavy ion plasma source during storms. In addition, the MHD simulation is a single-fluid and therefore does not contain energetic ring current particles; particles in this nonthermal part of the distribution can carry much of the energy density in the inner magnetosphere during storm time. We note that sunward $E \times B$ drifts create some pressure pile up in the inner magnetosphere in the MHD simulation. However, only gradient and curvature B drifts can support and maintain a realistic, asymmetric ring current around Earth. A discussion of methods that can improve the performance of the MHD simulation in this regard follows next.

6. Discussion

[26] We have compared the MHD simulation with the Tsyganenko storm model and GOES data for a major storm event. The results show that both of these global models have their own strengths and weaknesses when predicting the storm-time inner magnetosphere. There are elements of the MHD code that work well, but others that do not, including the lack of realistic current systems. We have shown this to be a problem in this particular event. To identify if this is a recurrent problem in the LFM code when reproducing other storm or nonstorm intervals, we repeat the model and data comparison with more MHD results.

6.1. Statistical Study of Inner Magnetosphere MHD Simulations During Storms

[27] We simulated nine magnetic storm intervals using upstream solar wind measurements (Wind or ACE) and the standard simulation grid. We also simulated a 2-month, storm-free interval for comparison. The nine storm intervals include 14–18 May, 2–5 September, and 6–9 November 1997; 22–25 September and 21–24 October 1999; 6–9 April 2000; 21–25 October 2001; 16–20 April 2002; and the Sep98 event. These storms are representative of storms with Dst minima ranging from −98 to −318 nT, including three storms selected for study by the GEM community. For the 2-month storm-free simulation, we use Wind data from the interval between 23 February and 28 April 1996. There are two simulation gaps at the end of March and mid-April
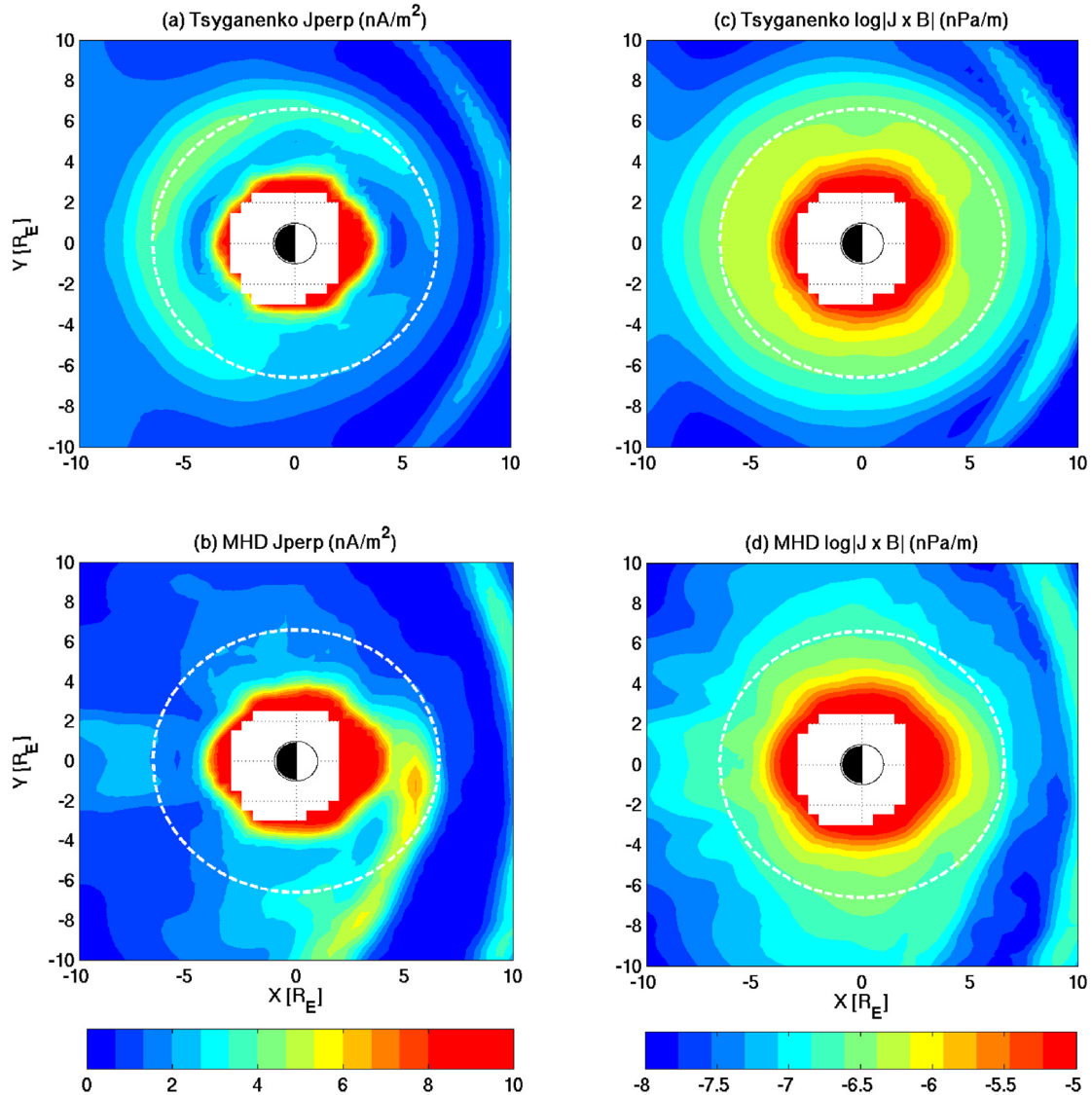
Figure 5. (a, b) Current systems and (c, d) plasma pressure gradient maps calculated from the T03 model and the MHD simulations at the equatorial plane during storm main phase, with a $1.5 \times 1.5\ R_E$ data smoothing. The white dashed lines denote the location of geosynchronous orbit.

due to Wind's perigee passes. There are always two GOES satellites in operational mode. We use all available GOES data in the statistical study.

[28] We extract the magnetic fields at the GOES position in geosynchronous orbit from the nine storm intervals as well as the 2-month simulation interval and compare with the GOES observations. To quantify this comprehensive time-series comparison, we bin the difference fields between the MHD outputs and GOES observations ($\Delta B = B_{MHD} - B_{GOES}$) according to GOES local time. The ΔB value chosen to quantify each local time bin is the median value of each bin. Figure 6 shows the binned residual fields (ΔB_x, ΔB_y, ΔB_z and elevation angle difference), sorted according to storm ($Dst < -20$ nT) and nonstorm ($Dst \geq -20$ nT) conditions.

[29] For nonstorm periods (red curves), the LFM code predicts the ΔB_x and ΔB_y (upper two panels, from left to right) components at geostationary orbit well within ± 10 nT

from the observed value at all local times. However, the simulated ΔB_z (lower left panel) component systematically deviates from these small values regardless of local time, ranging between about 10 nT on the dayside and 30 nT on the nightside. During stormy conditions (blue curves), the MHD predictions of B_x and B_z are consistently higher than observed, especially on the nightside. Again, the simulations predict the B_y component very well, with small residuals at all local times. The elevation angle comparison (lower right panel) shows that the MHD field lines are not stretched enough at all local times but especially for storm periods and in the midnight sector. As discussed in section 5, we believe this is mainly due to the lack of sufficiently realistic current systems in the MHD simulations, especially during major storm events and on the nightside. In the following sections, we discuss such constraints of the LFM code and several ways for improving the simulation predictive shortcomings quantified in Figure 6.
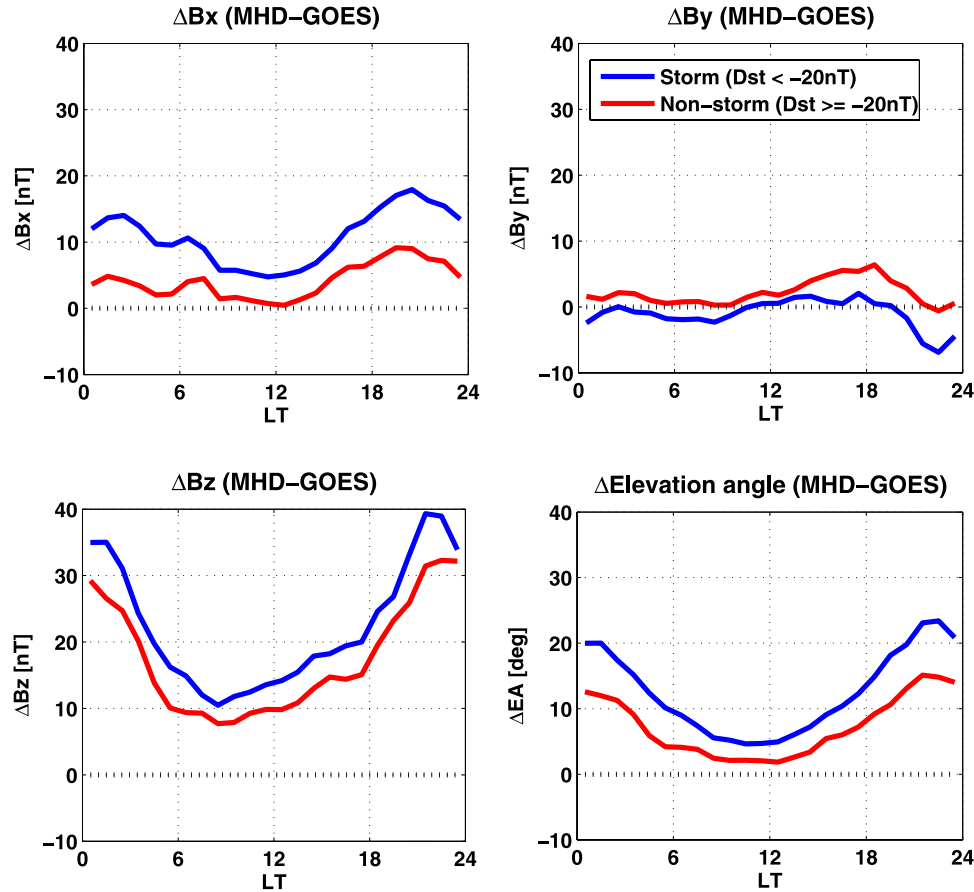
Figure 6. Quantitative comparisons of the MHD simulations with GOES observations for nine magnetic storm intervals and a two-month storm-free interval. The binned residual fields (ΔB_x, ΔB_y, ΔB_z and elevation angle difference) are sorted according to storm (blue curves, $Dst < -20$ nT) and non-storm (red curves, $Dst \geq -20$ nT) conditions.

## 6.2. Pathways to Improve the MHD Simulations

[30] In section 6.1 we confirmed and quantified systematic differences between the MHD predictions and observed properties of the inner magnetosphere. Global MHD codes are relatively sophisticated representations of the large-scale structure and dynamics of Earth's magnetosphere, but several factors limit model performance. For instance, the adapted grid cells of the LFM code may still be too large, leading to numerical diffusion which affects the simulation results. In addition, the single-fluid MHD simulations necessarily fail to describe the energy-dependent inner magnetosphere where gradient and curvature B drifts become important, particularly during storm times. $E \times B$ drifts carry plasma pressure inward to the inner magnetosphere region to establish a weak ring current. However, lack of the gradient and curvature B drifts in combination with the frozen-in flux condition in the MHD code, result in unsustainable realistic pressure gradients. In addition, the lack of mass transport between the magnetosphere and the ionosphere, such as ionospheric outflow and electron precipitation, may alter the simulation results significantly. Polar and FAST satellites both observed intense ionospheric outflows during the Sep98 event [*Moore et al.*, 1999; *Strangeway et al.*, 2000]. A multifluid MHD code could quantify the contributions of an ionospheric plasma source

using the same computational scheme as in the single-fluid model. Sparse knowledge of global ionospheric outflow characteristics limits attempts to include such effects in MHD codes, so we defer further discussion of this topic. Next, we assess the first two possible steps that may help improve simulation results: grid resolution and drift physics.

6.2.1. Increased LFM Code Grid Resolution

[31] To test how the MHD grid resolution affects the simulation result, we run the Sep98 storm again but with a higher resolution computational grid. For the standard MHD run, the grid size at geosynchronous orbit is between 0.3 and 0.5 R_E. The higher resolution grid doubles the cell numbers in both the radial and azimuthal directions, and keeps the cell numbers in the polar direction the same, yielding grid sizes of 0.15 R_E on the dayside and 0.25 R_E on the nightside. Increasing simulation resolution reduces the numerical diffusion between the grid cells particularly important where sharp spatial gradients exist. When grid resolution is increased, the gyroradius of a representative plasmasheet proton can occasionally approach the simulation scale at localized points in the far tail (>40 R_E). While this might be of concern for tail physics, it will not affect our study of the inner magnetosphere.

[32] In Figures 7 and 8 we show simulation results from both the standard and the double resolution MHD runs
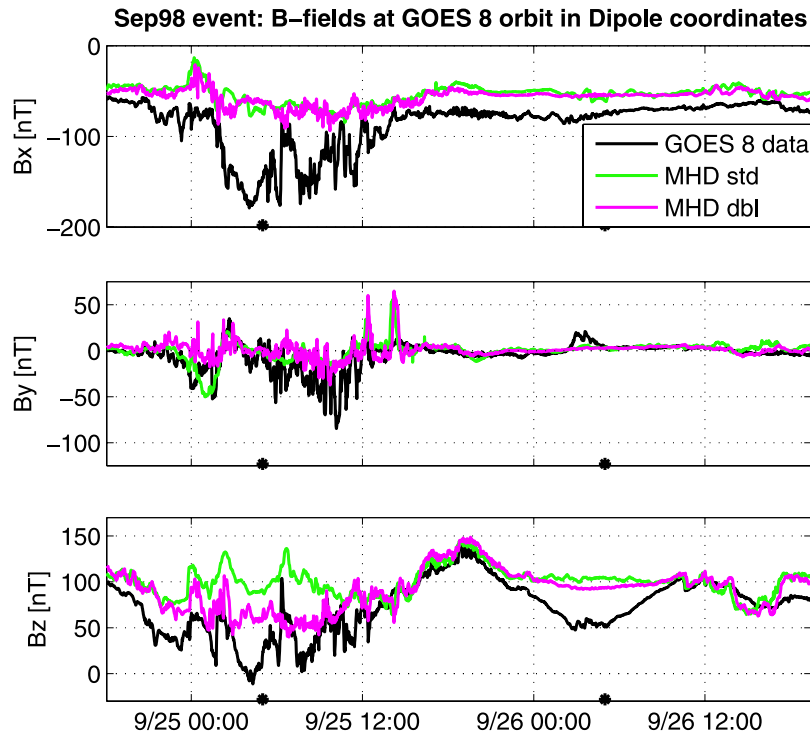
Figure 7. Comparisons of both the standard and the double resolution MHD results and the GOES 8 field measurements. The black lines are measurements from GOES 8. The green and magenta lines are the MHD predicted results from the standard and the double resolution grids at the GOES 8 positions.

compared with the GOES 8 and GOES 10 data. The higher resolution MHD run (magenta curves) predicts the B_z component better than the standard run, with reduced field strengths on the nightside during stormy conditions. It also better reproduces the very fine timescale variations observed in the B_x and B_y components. On the other hand, the higher resolution run predicts the magnitude of B_x and B_y nearly identically to the standard resolution run. Table 1 shows the relative improvement of the double resolution MHD run, compared to the standard resolution run and
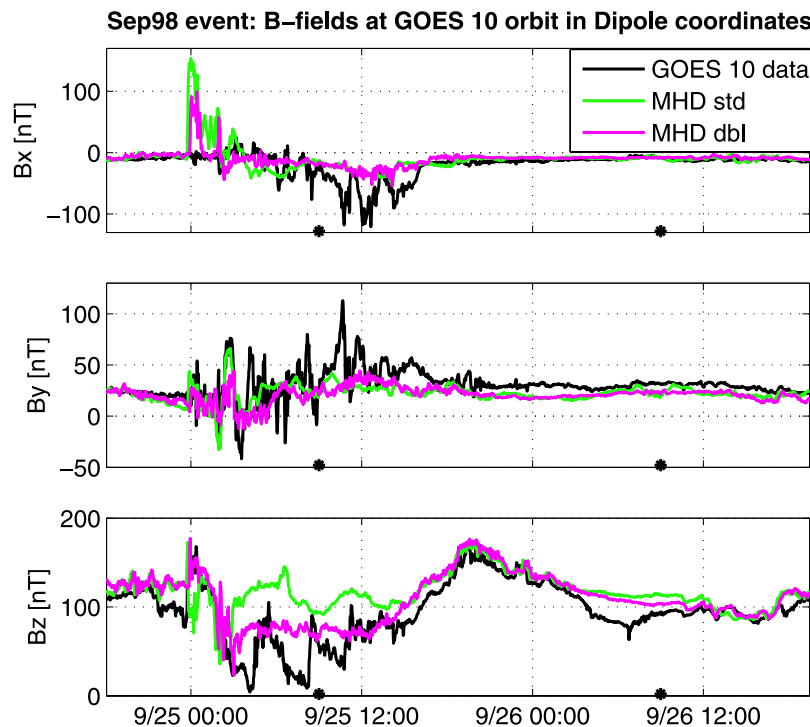
Figure 8. The same comparison as Figure 7 using GOES 10 data.

Table 1. Root-Mean-Square (RMS) Difference Between the Observed Magnetic Field and That Predicted by MHD Standard and Double Resolution Runs, and the Tsyganenko 2003 Model, on the GOES 8 and 10 Orbit During the Sep98 Event

	RMS			
	B_x	B_y	B_z	$|B|$
GOES 8 Orbit				
MHD standard	37	13	39	19
MHD double	40	14	26	26
T03 model	13	19	18	14
GOES 10 Orbit				
MHD standard	25	16	35	27
MHD double	19	16	21	18
T03 model	16	15	16	18

Tsyganenko 2003 model. We calculate the root-mean-square difference between the observed magnetic field and that predicted by models in vector components and magnitudes for both GOES 8 and 10 orbits during the Sep98 storm.

[33] Ideally, increased model grid resolution in the MHD simulations should provide better predictive results. However, computation time scales as the fourth power of the spatial resolution improvement. Higher resolution runs thus become more expensive and at some point become impractical for model users.

[34] Increasing cell resolution in the simulations will improve model performance only to a certain level. Increasing resolution yields diminishing returns when the spatial gradients inherent to the modeled physics are already well resolved. At some point, only including the full drift physics in the code can help the MHD simulations reproduce a more realistic storm-time magnetosphere. Figures 7 and 8 suggest that additional physics, in addition to increased spatial resolution, are required.

6.2.2. Coupling LFM With a Drift Physics Ring Current Model

[35] The ongoing effort of coupling the global MHD codes and the Rice Convection Model (RCM) [*Harel et al.*, 1981] should yield a better predictive representation of Earth's inner magnetosphere [*Toffoletto et al.*, 2004; *De Zeeuw et al.*, 2004]. Lack of magnetic field stretching in global MHD codes has been a known problem and was first addressed by *De Zeeuw et al.* [2004], who coupled the RCM to the BATSRUS global MHD code. Simulations of idealized mildly disturbed events [*De Zeeuw et al.*, 2004; *Toth et al.*, 2005] showed increased stretching of magnetic field lines in the magnetotail. Similar results were earlier found with the coupled RCM-Equilibrium Code, where the magnetic field is adjusted to maintain force equilibria with the RCM-computed pressures [*Toffoletto et al.*, 2001].

[36] The RCM is an inner magnetosphere model that computes particle drifts, currents, and electric fields assuming an isotropic pitch angle distribution of particles on closed magnetic field lines. This multifluid code includes energy-dependent transport of magnetospheric particles owing to gradient and curvature B drifts. At geosynchronous orbit, the RCM ionospheric grid cells, when mapped out along magnetic field lines from the ionosphere to the equatorial region, are less than 0.1 R_E in the perpendicular dimensions, which is finer than even the double-resolution

LFM grid. The main weakness of RCM is the use of preexisting external global magnetic fields as model inputs, fields that are not consistent with the computed particle pressure. In the fully coupled LFM/RCM code, LFM will provide RCM with magnetic fields that are consistent with the MHD momentum equation. RCM will perform drift physics in these fields to provide realistic plasma pressure and density, fed back to the MHD code, which may cause a significant inflation of the magnetic field, mostly on the nightside. Much of the mechanics of this coupling is described conceptually by *Toffoletto et al.* [2004].

[37] Successful coupling between a global MHD code and the RCM has been reported by the Michigan group [*De Zeeuw et al.*, 2004; *Toth et al.*, 2005]. LFM/RCM coupling is still in development and is not yet ready to run real event studies. Instead, we perform a comparison of presently available coupled LFM/RCM and LFM-only results using idealized inputs. We assess the effect of the ring current by running both models with identical inputs: solar wind density of 5 cm^{-3} and a solar wind speed of 400 km/s aligned along the X direction. Both the IMF B_x and B_y components are zero throughout the run. We start the run with an IMF B_z of -5 nT for a couple of hours, and then switch the IMF northward for an hour, then switch it back to southward for the rest of the run. This yields a weakly energized magnetosphere with an inferred *Dst* of ~-15 nT, as predicted by the model of [*Temerin and Li*, 2002]. The current version of the RCM used in the LFM assumes a zero dipole tilt; a new version that eliminates this assumption is under development [*Wolf et al.*, 2006]. Unlike the LFM alone, in the coupled LFM/RCM code results, plasma pressure builds up around Earth and forms a complete but weak ring current at the end of the simulation. Figure 9
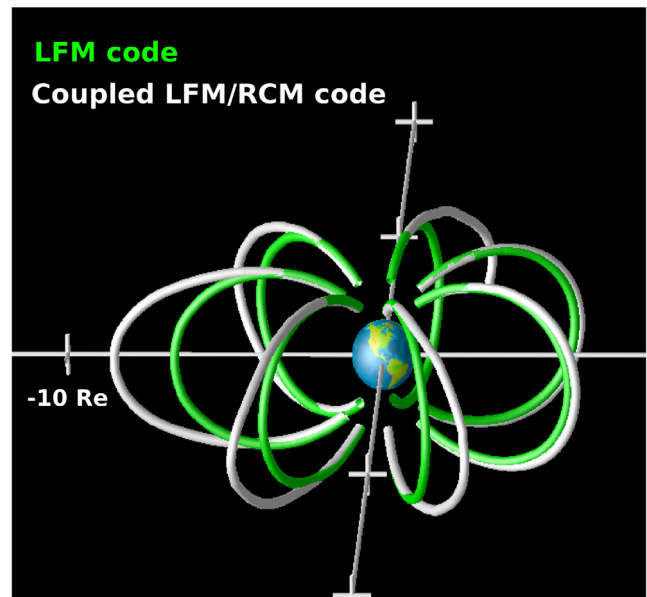
Figure 9. Magnetic field configurations of the LFM-only (green lines) and the coupled LFM/RCM (white lines) codes viewed from dawn at an angle above the equator. The field lines are traced from points starting at 2 R_E radius, geomagnetic latitude of 67 degrees, and at seven equispaced local times.

compares magnetic field topology between the LFM-only (green) and the LFM/RCM (white) results. The field lines are traced from points starting at 2 R_E radius, geomagnetic latitude of 67 degrees, and at seven equispaced local times. The current systems in the LFM/RCM code stretches out field lines at all local times compared to the LFM-only run, especially on the nightside. The B_z field residuals between the two codes ($\Delta B_z = B_{z,LFM} - B_{z, LFM/RCM}$) are ~10 nT at noon and ~45 nT at midnight, comparable to the field residuals between LFM-only and GOES data for nonstorm condition (see Figures 5 and 6). This suggests that the LFM/RCM coupled code will reproduce the non-storm-time inner magnetosphere much better by including the essential drift physics. This preliminary result is promising, though more investigations are required before reaching firm conclusions, especially during storm conditions.

7. Conclusions and Summary

[38] Our study compared LFM MHD code results with the Tsyganenko 2003 storm model and the GOES observations in order to understand the storm-time configuration of the inner magnetosphere and the performance of global MHD simulations. The physics needed to describe fully the evolution of the inner magnetosphere magnetic fields and plasma during magnetic storms is complicated and difficult to simulate. The limitations of global MHD codes, such as not including important nonideal MHD physics, underspecified initial and boundary conditions, and demand on computational resources, constrain their ability to reproduce the time-dependent magnetosphere accurately. Therefore it is important to validate the MHD simulations with observations to understand and quantify the practical limits of the global codes [*Ridley et al.*, 2002; *Spence et al.*, 2004].

[39] We note that the Tsyganenko 2003 storm model overall reproduces the magnetic field at geosynchronous orbit very well throughout the entire Sep98 storm. The greatest difference between the model prediction and data is ~50 nT during storm main phase, but with differences generally much lower. The T03 model predicts the geosynchronous fields better than the MHD simulations even for several storm events not included in T03 model data set. However, the Tsyganenko models are temporally and spatially averaged views of the dynamic magnetosphere, so they do not reproduce small timescale field variations as well as the MHD simulations. Even though constructed from sparse satellite data in time and space, the T03 model describes the storm-time field configuration of the inner magnetosphere with impressive success. Nevertheless, outside the model spatial domain and during extreme conditions, model users should use it with caution. In regions and conditions of validity, the T03 model provides useful baseline predictions of the inner magnetosphere to evaluate the accuracy of MHD simulations.

[40] We explored LFM model performance through case study analysis. During the September 1998 storm (*Dst* minimum of −213 nT) both the LFM code and the Tsyganenko model predict well the magnetic field strength and basic variations throughout the event, when compared with the observed fields from the GOES 8 and 10 satellites. The T03 model predicts the magnetic field better than the

MHD simulation in B_x and B_z components. However, the LFM code better simulates the more rapid magnetic field fluctuations that result from variable solar wind driver inputs. Comparing the magnetic field configurations, the T03 modeled field lines stretch more than the MHD simulated field lines, particularly on the nightside and during the storm main phase. Pressure gradient maps (inferred from maps of $J \times B$) show that the MHD simulation has an insufficient current system in the inner magnetosphere and overestimates the field strength (by as much as ~100 nT in the B_z component) during storm main phase.

[41] To assess whether features seen in the case study are persistent trends, we also performed statistical comparisons. In our statistical study, we compared the MHD results of nine magnetic storms and a 2-month-long simulation with geosynchronous satellite measurements. For nonstorm periods ($Dst \geq -20$ nT), the MHD simulated magnetic fields in the X and Y components are comparable to the observed fields, being well within ±10 nT. The simulated Z component systematically differs from observations by ~10 nT on the dayside and ~30 nT on the nightside. Under storm conditions ($Dst < -20$ nT), the residual fields between the simulations and observations follow the same trends but are even larger, especially on the nightside.

[42] These statistical results suggest that the lack of a sufficient inner magnetosphere current system in the LFM could be the source for the model/data discrepancy for all solar wind conditions and local times. We discussed two other known limiting factors of the simulations and explored their effects. First, increasing the simulation spatial resolution will reduce possible numerical diffusion occurring between cells in regions of sharp gradients, such as the inner magnetosphere during storms. We find that a high spatial resolution run develops greater plasma pressure in the inner magnetosphere and also reduces the B_z strength by ~50 nT during storm main phase, both partial improvements of model predictability. Second, we assess the importance of drift physics effects in the ring current region by comparing the LFM code with and without these non-MHD features included. Using preliminary results from an ongoing coupling effort of the LFM and RCM models, we find that with non-MHD features included the plasma pressure increases significantly and the magnetic field lines become more stretched. Both quantitative changes are needed for improved comparison with observations.

References

Birn, J., et al. (2001), Geospace Environmental Modeling (GEM) magnetic reconnection challenge, *J. Geophys. Res.*, *106*, 3715–3720.
Boris, J. P. (1970), A physically motivated solution of the Alfven problem, NRL Memo. Rep., Naval Res. Lab., Washington, D. C.
De Zeeuw, D. L., S. Sazykin, R. A. Wolf, T. I. Gombosi, A. J. Ridley, and G. Toth (2004), Coupling of a global MHD code and an inner magnetospheric model: Initial results, *J. Geophys. Res.*, *109*, A12219, doi:10.1029/2003JA010366.

Elkington, S. R., M. Wiltberger, A. A. Chan, and D. N. Baker (2004), Physical models of the geospace radiation environment, *J. Atmos. Sol. Terr. Phys.*, 66, 1371–1387.

Fedder, J. A., S. P. Slinker, J. G. Lyon, C. T. Russell, F. R. Fenrich, and J. G. Luhmann (1997), A first comparison of POLAR magnetic field measurements and magnetohydrodynamic simulation results for field-aligned currents, *Geophys. Res. Lett.*, 24, 2491–2494.

Goodrich, C. C., M. Wiltberger, R. E. Lopez, K. Papadopoulos, and J. G. Lyon (1998), An overview of the impact of the January 10–11, 1997 magnetic cloud on the magnetosphere via global MHD simulation, *Geophys. Res. Lett.*, 25, 2537–2540.

Guild, T., H. E. Spence, L. Kepko, M. Wiltberger, C. Goodrich, J. Lyon, and W. J. Hughes (2004), Plasma sheet climatology: Geotail observations and LFM model comparisons, *J. Atmos. Sol. Terr. Phys.*, 66, 1351–1360.

Harel, M., R. A. Wolf, P. H. Reiff, R. W. Spiro, W. J. Burke, F. J. Rich, and M. Smiddy (1981), Quantitative simulation of a magnetospheric substorm: 1. Model logic and overview, *J. Geophys. Res.*, 86, 2217–2241.

Janhunen, P., and A. Huuskonen (1993), A numerical ionosphere-magnetosphere coupling model with variable conductivities, *J. Geophys. Res.*, 98, 9519–9530.

Lui, A. T. Y., H. E. Spence, and D. P. Stern (1994), Empirical modeling of the quite time nightside magnetosphere, *J. Geophys. Res.*, 99, 151–158.

Lyon, J. G., J. A. Fedder, and C. M. Mobarry (2004), The Lyon-Fedder-Mobarry (LFM) global MHD magnetospheric simulation code, *J. Atmos. Sol. Terr. Phys.*, 66, 1333–1350.

Moldwin, M. B., L. Downward, H. K. Rassoul, R. Amin, and R. R. Anderson (2002), A new model of the location of the plasmapause: CRRES results, *J. Geophys. Res.*, 107(A11), 1339, doi:10.1029/2001JA009211.

Moore, T. E., et al. (1999), Ionospheric mass ejection in response to a CME, *Geophys. Res. Lett.*, 26, 2339–2342.

Ogino, T., R. J. Walker, and M. Ashour-Abdalla (1994), A global magnetohydrodynamics simulation of the response of the magnetosphere to a northward turning of the interplanetary magnetic field, *J. Geophys. Res.*, 99, 11,027–11,042.

Powell, K. G., P. L. Roe, T. J. Linde, T. I. Gombosi, and D. L. DeZeeuw (1999), A solution-adaptive upwind scheme for ideal magnetohydrodynamics, *J. Comput. Phys.*, 154, 284, doi:10.1006/jcph.1999.6299.

Pulkkinen, T. I. (2001), How to address the accuracy of empirical magnetic field models?, *Adv. Space Res.*, 28, 1717–1726.

Pulkkinen, T. I., and M. Wiltberger (2000), Thin current sheet evolution as seen in observations, empirical models and MHD simulations, *Geophys. Res. Lett.*, 27, 1363–1366.

Raeder, J. (1999), Modeling the magnetosphere for northward interplanetary magnetic field: Effects of electrical resistivity, *J. Geophys. Res.*, 104, 17,357.

Raeder, J. R. L. M., L. A. Frank, S. Kokubun, G. Lu, T. Mukai, W. R. Paterson, J. B. Sigwarth, H. J. Singer, and J. A. Slavin (2001), Global simulation of the Geospace Environment Modeling substorm challenge event, *J. Geophys. Res.*, 106, 381–396.

Reeves, G. D., R. H. W. Friedel, S. Bourdarie, M. F. Thomsen, S. Zaharia, M. G. Henderson, Y. Chen, V. K. Jordanova, B. J. Albright, and D. Winske (2005), Toward understanding radiation belt dynamics, nuclear explosion-produced artificial belts, and active radiation belt remediation: Producing a radiation belt data assimilation model, in *Inner Magnetosphere Interactions: New Perspectives From Imaging*, vol. 159, edited by J. Burch, M. Schulz, and H. Spence, pp. 221–235, AGU, Washington, D.C.

Ridley, A. J., K. C. Hansen, G. Toth, D. L. D. Zeeuw, T. I. Gombosi, and K. G. Powell (2002), University of Michigan MHD results of the Geospace Global Circulation Model metrics challenge, *J. Geophys. Res.*, 107(A10), 1290, doi:10.1029/2001JA000253.

Spence, H., M. G. Kivelson, and R. J. Walker (1987), Static magnetic field models consisten with nearly isotropic plasma pressure, *Geophys. Res. Lett.*, 14, 872–875.

Spence, H., D. Baker, A. Burns, T. Guild, C.-L. Huang, G. Siscoe, and R. Weigel (2004), Center for integrated space weather modeling metrics plan and initial model validation results, *J. Atmos. Sol. Terr. Phys.*, 66, 1499–1507.

Strangeway, R. J., C. T. Russell, C. W. Carlson, J. P. McFadden, R. E. Ergun, M. Temerin, D. M. Klumpar, W. K. Peterson, and T. E. Moore (2000), Cusp field-aligned currents and ion outflows, *J. Geophys. Res.*, 105, 21,129–21,142.

Tanaka, T. (2003), Formation of magnetospheric plasma population regimes coupled with the dynamo process in the convection system, *J. Geophys. Res.*, 108(A8), 1315, doi:10.1029/2002JA009668.

Temerin, M., and X. Li (2002), A new model for the prediction of Dst on the basis of the solar wind, *J. Geophys. Res.*, 107(A12), 1472, doi:10.1029/2001JA007532.

Thomsen, M. F., D. J. McComas, G. D. Reeves, and L. A. Weiss (1996), An observational test of the Tsyganenko (T89a) model of the magnetospheric field, *J. Geophys. Res.*, 101, 24,827–24,836.

Toffoletto, F. R., J. Birn, M. Hesse, R. W. Spiro, and R. A. Wolf (2001), Modeling inner magnetospheric electrodynamics, in *Space Weather*, *Geophys. Monogr. Ser.*, vol. 125, edited by P. Song, H. Singer, and G. Siscoe, p. 265, AGU, Washington, D. C.

Toffoletto, F. R., S. Sazykin, R. W. Spiro, R. A. Wolf, and J. G. Lyon (2004), RCM meets LFM: initial results of one-way coupling, *J. Atmos. Sol. Terr. Phys.*, 66, 1361–1370.

Toth, G., et al. (2005), Space Weather Modeling Framework: A new tool for the space science community, *J. Geophys. Res.*, 110, A12226, doi:10.1029/2005JA011126.

Tsyganenko, N. A. (1987), Global quantitative models of the geomagnetic field in the cislunar magnetosphere for different disturbance levels, *Planet. Space Sci.*, 35, 1347–1358.

Tsyganenko, N. A. (1989), A magnetospheric magnetic field model with a warped tail current sheet, *Planet. Space Sci.*, 37, 5–20.

Tsyganenko, N. A. (1995), Modeling the Earth's magnetospheric magnetic field confined within a realistic magnetopause, *J. Geophys. Res.*, 100, 5599.

Tsyganenko, N. A. (2002a), A model of the near magnetosphere with a dawn-dusk asymmetry: 1. Mathematical structure, *J. Geophys. Res.*, 107(A8), 1179, doi:10.1029/2001JA000219.

Tsyganenko, N. A. (2002b), A model of the near magnetosphere with a dawn-dusk asymmetry: 2. Parameterization and fitting to observations, *J. Geophys. Res.*, 107(A8), 1176, doi:10.1029/2001JA000220.

Tsyganenko, N. A., and M. I. Sitnov (2005), Modeling the dynamics of the inner magnetosphere during strong geomagnetic storms, *J. Geophys. Res.*, 110, A03208, doi:10.1029/2004JA010798.

Tsyganenko, N. A., and A. V. Usmanov (1982), Determination of the magnetospheric current system parameters and development of experimental geomagnetic field models based on data from IMP and HEOS satellites, *Planet. Space Sci.*, 30(10), 985–998.

Tsyganenko, N. A., H. J. Singer, and J. C. Kasper (2003), Storm-time distortion of the inner magnetosphere: How severe can it get?, *J. Geophys. Res.*, 108(A5), 1209, doi:10.1029/2002JA009808.

White, W. W., J. A. Schoendorf, K. D. Siebert, N. C. Maynard, D. R. Weimer, G. L. Wilson, B. U. O. Sonnerup, G. L. Siscoe, and G. M. Erickson (2001), MHD simulation of magnetospheric transport at the mesoscale, in *Space Weather*, *Geophys. Monogr. Ser.*, vol. 125, edited by P. Song, H. J. Singer, and G. L. Siscoe, pp. 229–240, AGU, Washington, D. C.

Wiltberger, M., W. Wang, A. G. Burns, S. C. Solomon, L. G. Lyon, and C. C. Goodrich (2004), Initial results from the coupled magnetosphere ionosphere thermosphere model: Magnetospheric and ionospheric responses, *J. Atmos. Sol. Terr. Phys.*, 66, 1411–1423.

Winglee, R. M. (1998), Multi-fluid simulations of the magnetosphere: The identification of the geopause and its variation with IMF, *Geophys. Res. Lett.*, 25(24), 4441–4444.

Wolf, R. A., R. W. Spiro, S. Sazykin, F. R. Toffoletto, and T.-S. Huang (2006), Use of Euler potentials for describing magnetosphere-ionosphere coupling, *J. Geophys. Res.*, 111, A07315, doi:10.1029/2005JA011558.

Zaharia, S., and C.-Z. Cheng (2003), Can an isotropic plasma pressure distribution be in force balance with the T96 model field?, *J. Geophys. Res.*, 108(A11), 1412, doi:10.1029/2002JA009501.

———————————

C.-L. Huang and H. E. Spence, Center for Space Physics, Boston University, 725 Commonwealth Avenue, Boston, MA 02215, USA. (hcl@bu.edu)

J. G. Lyon, Department of Physics and Astronomy, Dartmouth College, 6127 Wilder Laboratory, Hanover, NH 03755, USA.

S. Sazykin and F. R. Toffoletto, Physics and Astronomy Department, Rice University, 6100 Main Street, Houston, TX 77005, USA.

H. J. Singer, Space Enivroment Center, NOAA, 325 Broadway, Boulder, CO 80305, USA.